6
Numerical examples

In the following, some numerical examples are presented in order to validate the formulations proposed in the previous chapters of finite, infinite and halfspace problems. The boundary element methods for axisymmetric problems were programmed in FORTRAN 90/95, for linear and quadratic elements. The numbers of integration points used in the Gauss-Legendre and the logarithmic weighted Gauss quadrature rules are 6 and 8, respectively.

For each example, one compares displacements along the boundary as well as displacements and stresses at internal points in the domain with the corresponding analytical solutions. A relative error is presented,

$$\text{Error} = \sqrt{\frac{\sum (x_{a_i} - x_{n_i})^2}{\sum x_{a_i}^2}} \tag{6-1}$$

where x_a are the analytical results, x_n are the numerical results and the summation index i refers to the number of results being analyzed.

The abbreviations used in the following tables and graphics are, regarding the formulation,

- Analytical: Analytical solution;
- BEM: Conventional Boundary element method (Section 3.1.3);
- KBEM: Boundary element method using a stiffness matrix and equivalent nodal forces (Section 3.1.4);
- SHBEM: Simplified-hybrid boundary element method;

and regarding the fundamental solution employed,

- F: Fullspace fundamental solution;
- H: Halfspace fundamental solution.

6.1
Examples for finite domains

6.1.1
Disc under axial compression

A disc of radius $R = 10$ m, thickness $e = 1$ m, shear modulus $\mu = 12$ MPa and Poisson's ratio $\nu = 0.25$, as depicted in Fig. 6.1, is submitted to a distributed axial compressive load $t = -300$ N/m along the boundary segments AB and CD.

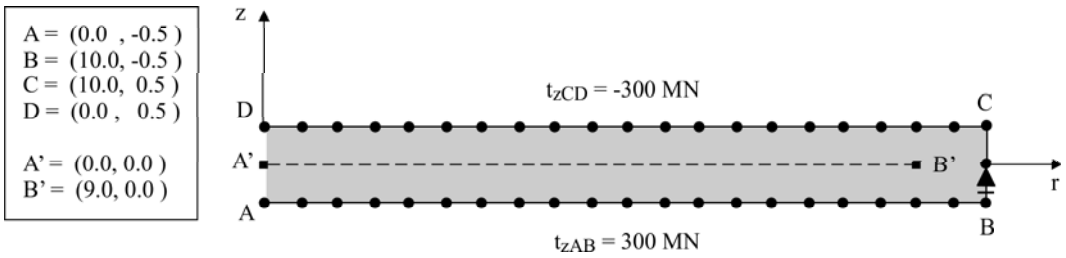

Figure 6.1: Boundary element model of a disc subjected to axial compression

The analytical solution for this problem is [89]

$$u_r = -\frac{\nu\, r}{2\mu\,(1+\nu)}\,t, \quad u_z = \frac{z}{2\mu\,(1+\nu)}\,t,$$
$$\sigma_{rr} = 0, \quad \sigma_{rz} = 0 \quad \text{e} \quad \sigma_{zz} = t \tag{6-2}$$

in which t positive means tensile traction loads.

The problem was analyzed by a model with 43 nodes, as shown in Fig. 6.1. For the sake of conciseness, the results are presented only for meshes of quadratic elements. However, linear elements and more discretized meshes were also employed to check convergence of results. When a quadratic element has one extremity node on the axis of axisymmetry and the value $n_r = 0$ of the r-projection of the outward normal, the symmetric configuration of the element causes the equivalent nodal force for the node at $r = 0$ to be equal to zero, according to the analytical solutions presented in Section 4.1.5.3. Then, to make possible to evaluate the submatrices of unknown coefficients of $\mathbf{U}^*$, one repositions the middle node of this element to the coordinate $r = 0.51$, a perturbation sufficient to generate non-trivial equivalent nodal forces.

Although one is dealing with a convex domain, the geometry is symmetric in relation to a horizontal plane and, as a consequence, the basis $\mathbf{V}$ given in Section 4.1.3 has zero coefficient for the r-direction at node 22, between points B and C, as shown in Fig. 6.2. Also, the small values of $\mathbf{V}$ in the r-direction at

the first and last nodes are due to their position on the axis of axisymmetry and the value of $n_r = 0$ on their corresponding elements. Then, this problem cannot be dealt with in the frame of the initial proposition of Section 4.1.4. On the other hand, one achieved good accuracy in the results by the simplified boundary element method (SHBEM-F), thanks to the new procedure proposed in Section 4.1.5 for the evaluation of the unknown coefficients of the matrix $\mathbf{U}^*$, which is no longer affected by the behavior of the basis $\mathbf{V}$.

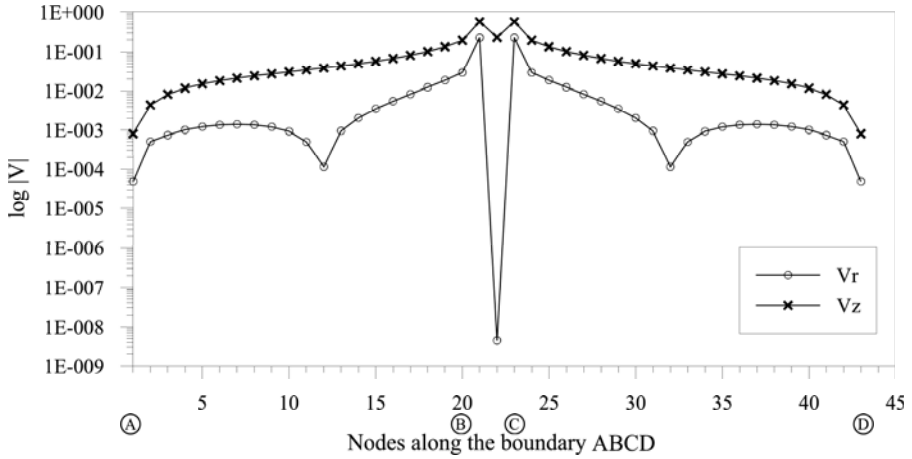

Figure 6.2: Basis $\mathbf{V}$ along the boundary ABCD

The results of displacements along the boundary are plotted in Fig. 6.3. Displacements and stresses, given in Fig. 6.1.1, were evaluated at 10 points equally spaced along the segment A'B'. Table 6.1 presents the global relative errors for the displacements and stress evaluated along the boundary and in the domain.

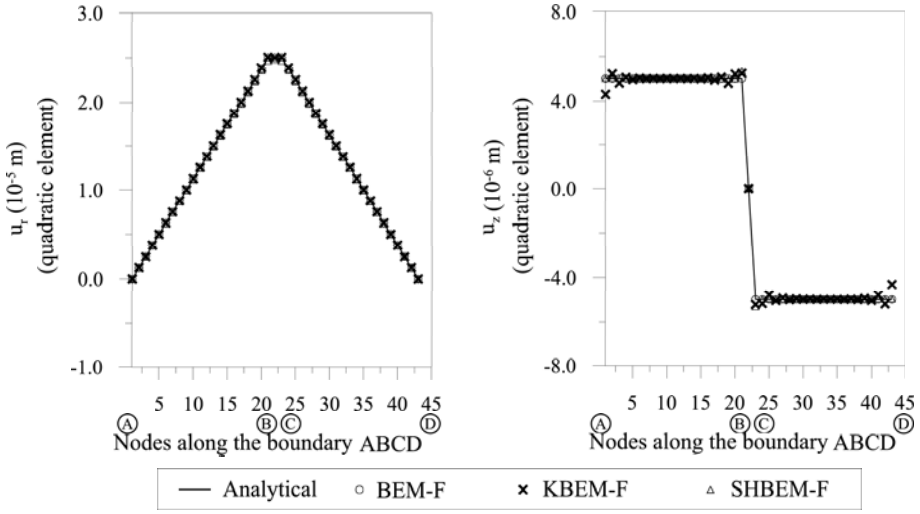

Figure 6.3: Displacements along the boundary ABCD

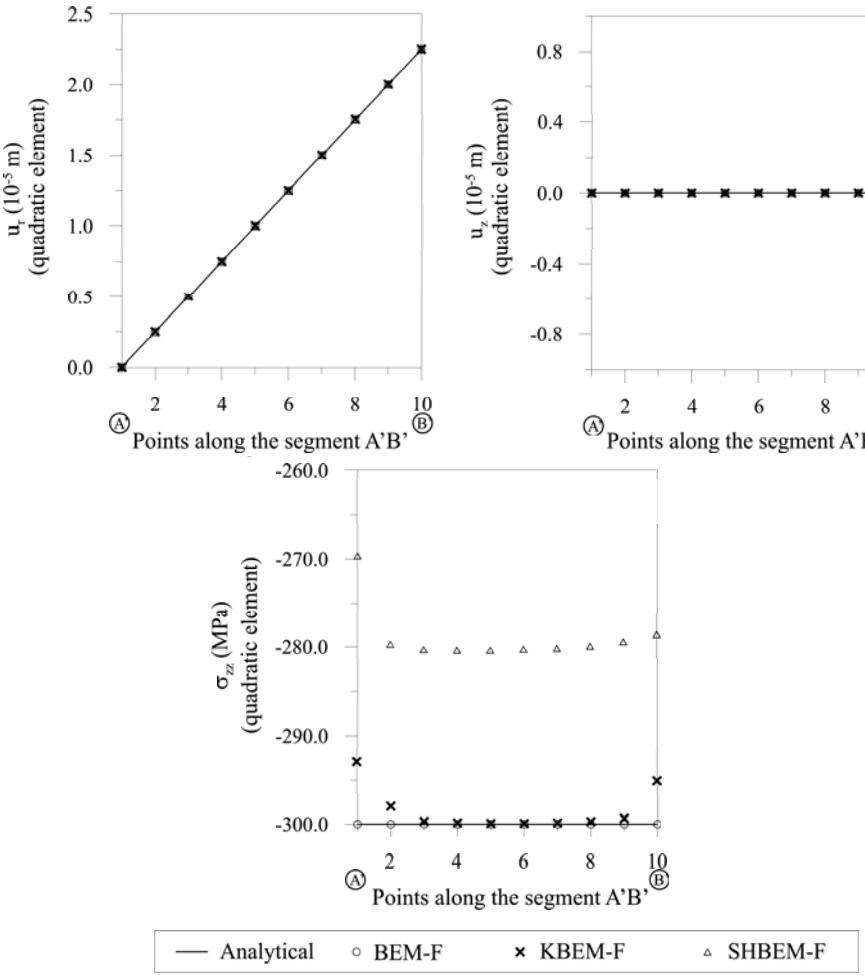

Figure 6.4: Displacements and stresses along the segment A'B'

Table 6.1: Global errors of the results found to a disc subjected to axial compression

	Error (%)				
Method	*Along the boundary*		*In the domain*		
	u_r	u_z	u_r	u_z	σ_{zz}
BEM-F	0.00	0.01	0.00	0.01	0.00
KBEM-F	0.21	3.72	0.10	0.01	0.93
SHBEM-F	0.95	1.48	0.12	0.09	7.12

Notice that the discontinuity in the traction forces at points B and C of the boundary cannot be correctly described by the equivalent nodal forces (which also occurs in the frame of the displacement finite element method). Since both the boundary and the simplified hybrid boundary element methods come from a stiffness matrix (KBEM-F and HSBEM-F, respectively), the corresponding results are less accurate in this example, such as for the displacements u_z along the boundary in Fig. 6.3 and stresses σ_{zz} along the segment A'B' in Fig. 6.1.1.

For this mesh, the results at the internal points shown in Fig. 6.1.1, obtained with the Somigliana's identity as used in the boundary element method (BEM-F),

are not affected by the distance of the internal points to the boundary elements (no *boundary-layer* effect observed). However, for the simplified-hybrid boundary element method (SHBEM-F), the internal points are too close to the boundary for evaluating the stresses σ_{zz} directly by just applying Eq. (4-2) without a correction, which resulted in a global relative error of 7.12%. In fact, as for the boundary element method in the case of quasi-singular integrals that arise for points close to the boundary [90], also in the simplified-hybrid boundary element method a specific procedure should be employed for evaluating results at internal points close to the boundary [46]. This technique was not applied in this work. However, one checked that, as the mesh is refined by duplicating the number of quadratric elements, the error for the stresses is reduced to 0.01%, of the same order of the error found for the boundary element method (BEM-F and KBEM-F), thus using an integral statement.

6.1.2
Disc submitted to radial tensile traction

Consider the same disc presented in the previous example, submitted to a distributed radial traction load $t = 300$ N/m along the boundary segment BC. The analytical solution for this problem is [89]

$$u_r = \frac{(1-\nu)\,r}{2\mu\,(1+\nu)}\,t, \quad u_z = -\frac{\nu\,z}{\mu\,(1+\nu)}\,t,$$
$$\sigma_{rr} = t, \quad \sigma_{rz} = 0 \quad \text{e} \quad \sigma_{zz} = 0 \tag{6-3}$$

where t positive means tensile traction loads.

The problem was analyzed with the same model of the previous example, shown in Fig. 6.5. The displacements along the boundary ABCD are shown in Fig. 6.6. The displacements and stresses along the segment A'B' are presented in Fig. 6.7. Table 6.2 presents the global relative errors for the displacements and stresses evaluated along the boundary and in the domain.

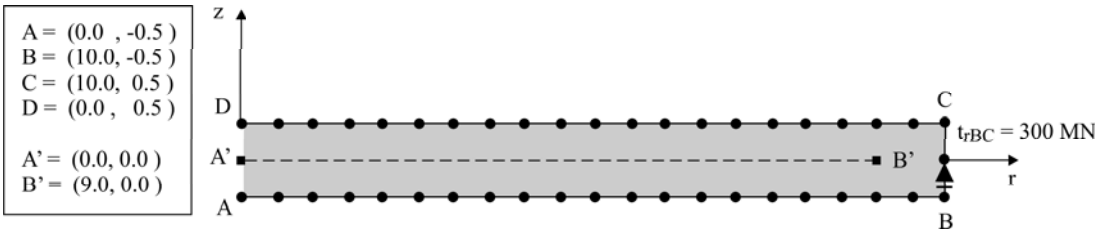

Figure 6.5: Boundary element model for a disc submitted to radial tensile traction

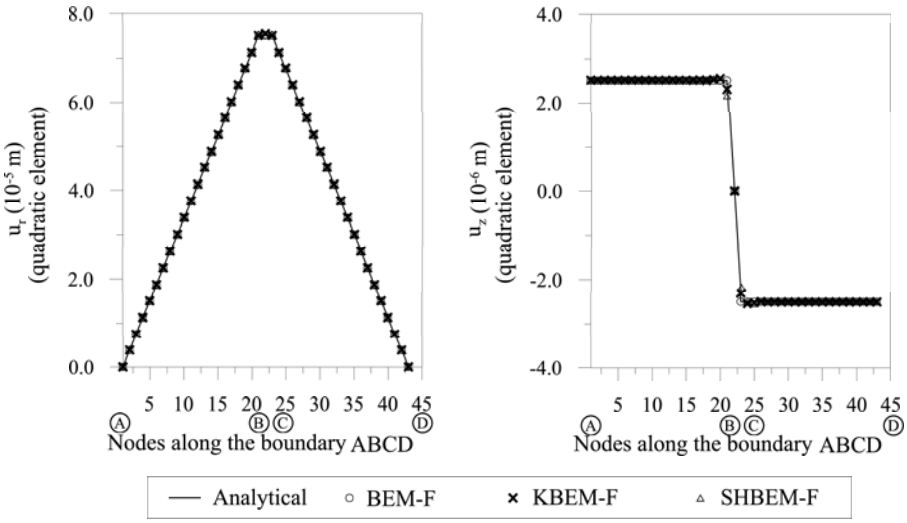

Figure 6.6: Displacements along the boundary ABCD

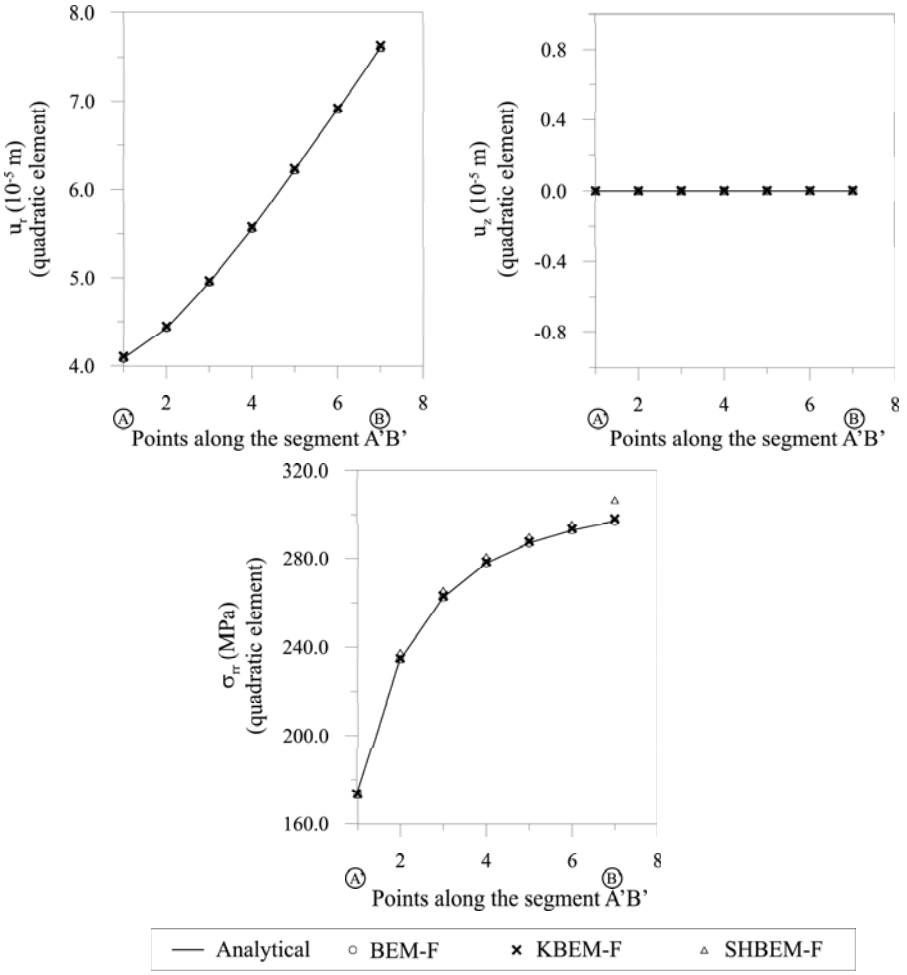

Figure 6.7: Displacements and stresses along the segment A'B'

Table 6.2: Global errors of the results found for a disc subjected to radial tensile traction

	Error (%)				
Method	*Along the boundary*		*In the domain*		
	u_r	u_z	u_r	u_z	σ_{rr}
BEM-F	0.00	0.03	0.00	0.08	0.00
KBEM-F	0.26	1.78	0.22	0.00	0.24
SHBEM-F	0.22	2.96	0.09	0.00	1.35

Also in these results, one may notice a small perturbation of displacements u_z along the portion BC of the boundary, as shown in Fig. 6.6, for both methods that make use of a stiffness matrix (KBEM-F and SHBEM-F). As in the previous example, the global relative error of 1.35% in stresses σ_{zz} for the simplified-hybrid boundary element method (SHBEM-F) is due to the proximity of the internal points to the boundary elements, which is not treated adequately in this work. On the other hand, the error for displacements present good accuracy when compared to the error for the boundary element method that makes use of a stiffness matrix (KBEM).

6.1.3
Hollow disc subjected to radial tensile traction

Consider a disc of external radius $R_e = 10$ m, internal radius $R_i = 2$ m, thickness $e = 1$ m, shear modulus $\mu = 12$ MPa and Poisson's ratio $\nu = 0.25$, as depicted in Fig. 6.8, submitted to a distributed radial tensile traction load $t = -300$ N/m along the boundary segment BC.

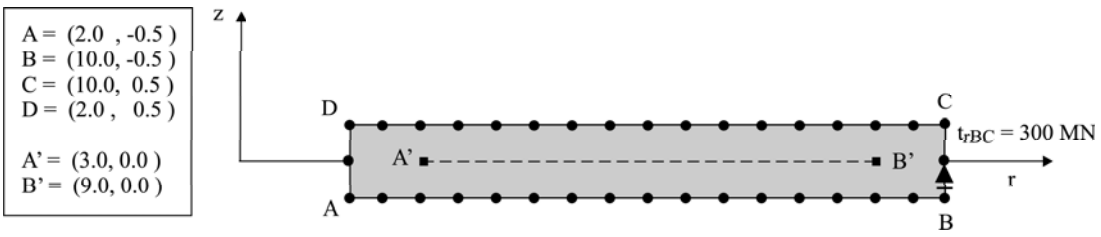

Figure 6.8: Boundary element model of a hollow disc subjected to radial tensile traction

The analytical solution for this problem is [89]

$$u_r = \frac{t}{2\mu(1-\nu)\, r\,(R_e^2 - R_i^2)} \left[(1+\nu)\, R_e^2\, R_i^2 + r^2\,(1-\nu)\, R_e^2\right]$$

$$u_z = -\frac{\nu\, R_e^2\, z\, t}{\mu\,(1-\nu)\,(R_e^2 - R_i^2)}$$

$$\sigma_{rr} = \frac{t}{r\,(R_e^2 - R_i^2)} \left[R_e^2\, R_i^2 - r^2\, R_e^2\right] \tag{6-4}$$

where t positive means tensile traction loads.

This problem was analyzed by a model with 36 nodes and quadratic elements, as shown in Fig. 6.8. As in the previous examples, since the problem is also symmetric in relation to a horizontal plane, the basis $\mathbf{V}$ given in Section 4.1.3 has zero coefficient in the r-direction at node 18, between the points B and C, as shown in Fig. 6.9. Moreover, as the domain is multiply-connected, the basis $\mathbf{V}$ also has zero coefficient in the r-direction at node 36, between points A and D. Again, despite these zero coefficients, one could achieve good accuracy in the results with the simplified boundary element method (SHBEM-F) by employing the procedure proposed in Section 4.1.5 for the evaluation of the unknown coefficients of the matrix $\mathbf{U}^*$.

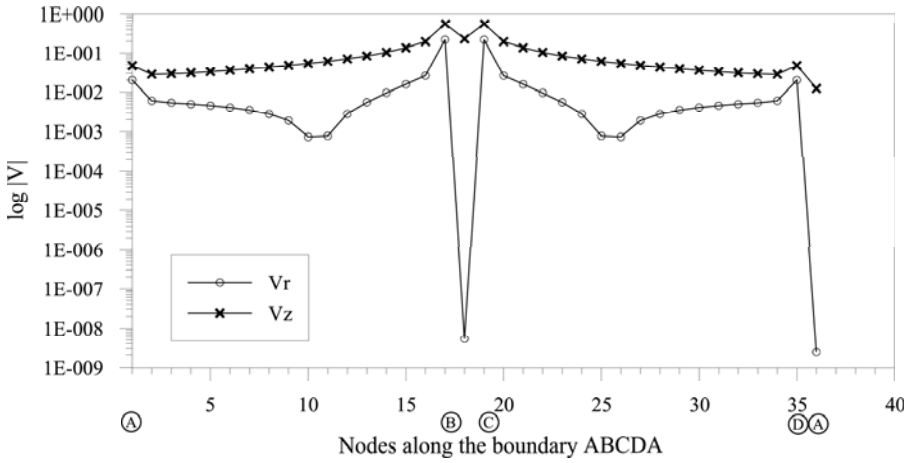

Figure 6.9: Basis $\mathbf{V}$ along the boundary ABCD

The results of displacement along the boundary are shown in Fig. 6.10. Also, displacements and stresses along 7 equally spaced points along the segment A'B' are given in Fig. 6.11. Table 6.3 presents the global relative errors for the displacements and stresses evaluated along the boundary and in the domain.

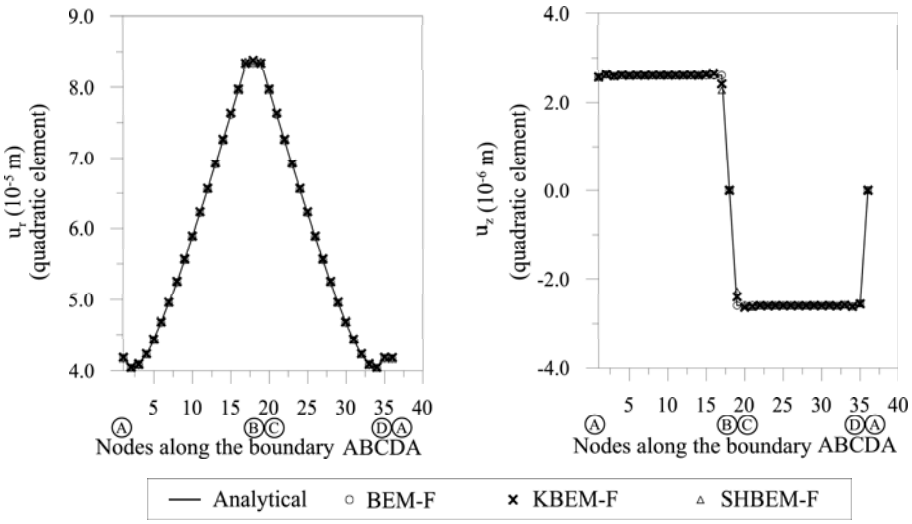

Figure 6.10: Displacements along the boundary ABCD

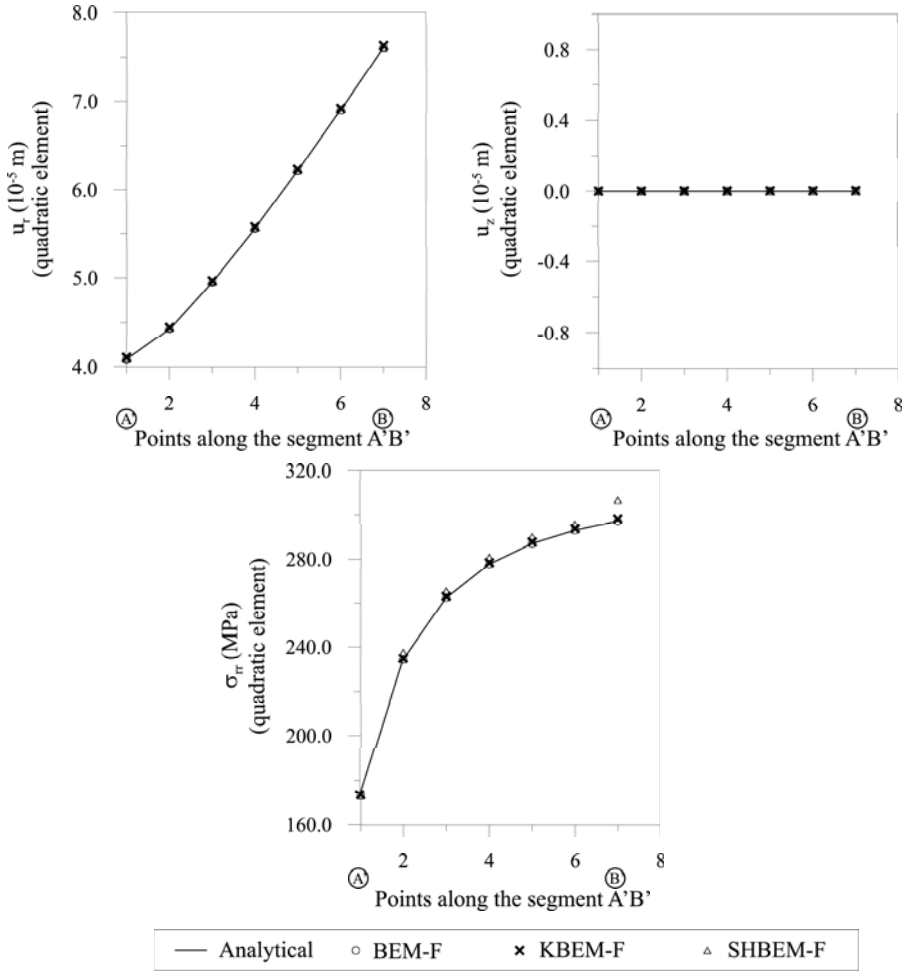

Figure 6.11: Displacements and stresses along the segment A'B'

Table 6.3: Global errors of the results found to a hollow disc subjected to radial tensile traction

	Error (%)				
Method	*Along the boundary*		*In the domain*		
	u_r	u_z	u_r	u_z	σ_{rr}
BEM-F	0.01	0.49	0.00	0.16	0.06
KBEM-F	0.25	1.95	0.23	0.25	0.24
SHBEM-F	0.04	3.19	0.02	0.02	1.69

Also in these results, one may notice a small perturbation of displacements u_z along the portion BC of the boundary, as shown in Fig. 6.10, for both methods that make use of a stiffness matrix (KBEM-F and SHBEM-F). As in the previous example, the global relative error of 1.69% in stresses σ_{zz} for the simplified-hybrid boundary element method (SHBEM-F) are due to the proximity of the internal points to the boundary elements, which is not treated adequately in this work. On the other hand, the error for displacements present good accuracy when compared to the error for the boundary element method that makes use of a stiffness matrix (KBEM).

6.1.4
Irregularly shaped, simply-connected domain subjected to a stress field

Consider a point force $\mathbf{p}^* \equiv (p_r^*, p_z^*) = (1, 1)$ MN applied at the coordinates P = $(10, -5)$ of a boundless elastic medium with shear modulus $\mu = 10$ MPa and Poisson's ratio $\nu = 0.3$. The displacement and stress fields produced at a point Q = (r, z) can be evaluated by directly applying the fullspace fundamental solution as

$$u_i = u_{ir}^{*\mathrm{f}}\, p_r^* + u_{iz}^{*\mathrm{f}}\, p_z^* \tag{6-5}$$

$$\sigma_{ij} = \sigma_{ijr}^{*\mathrm{f}}\, p_r^* + u_{ijz}^{*\mathrm{f}}\, p_z^* \tag{6-6}$$

where $u_{im}^{*\mathrm{f}}$ and $\sigma_{ijm}^{*\mathrm{f}}$ are given in Section 2.2. Now, let an irregular patch be drawn in this elastic medium, constituting a closed axisymmetric volume that does not contain the force $\mathbf{p}^*$ applied at point P, as depicted in Fig. 6.12. One can evaluate the displacements and traction forces along the boundary ABCDEF for $\mathbf{p}^*$ applied as described above, according to Eqs. (6-5) and (6-6). These results can be used as target values for comparison with the numerical simulations.

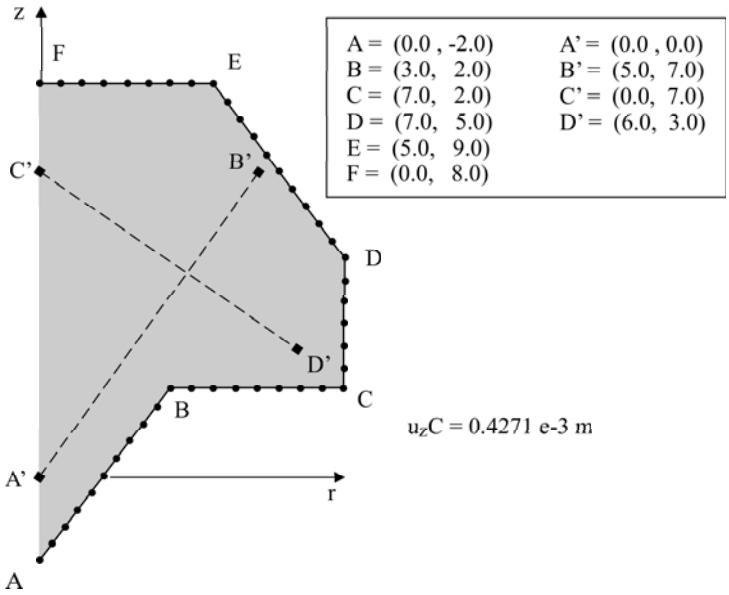

Figure 6.12: Boundary element model of an irregularly shaped, simply-connected domain subjected to a stress field

Consider the problem of the irregularly shaped domain, depicted in Fig. (6.12), subjected to traction forces along the boundary and prescribed displacement in the z-direction at C, obtained as above outlined. One solves the problem numerically for displacements and compares with the analytical expressions given by Eq. (6-5).

This problem was analyzed by a model with 43 nodes and quadratic elements, as depicted in Fig. 6.12. As in the example of Section 6.1.1, one repositions the middle node of the boundary element that contains the point F by a small perturbation, in order to generate nonzero equivalent nodal forces in the simplified-hybrid boundary element method.

As in the previous example of Section 6.1.1, the small values for the coefficients of $\mathbf{V}$ in the r-direction at the last node are due to its position on the axis of axisymmetry and the value of $n_r = 0$ on its corresponding element, as shown in Fig. 6.13. Again, despite these zero coefficient, one could achieve great accuracy in the results by the simplified boundary element method (SHBEM-F) by employing the procedure proposed in Section 4.1.5 for the evaluation of the unknown coefficients of $\mathbf{U}^*$.

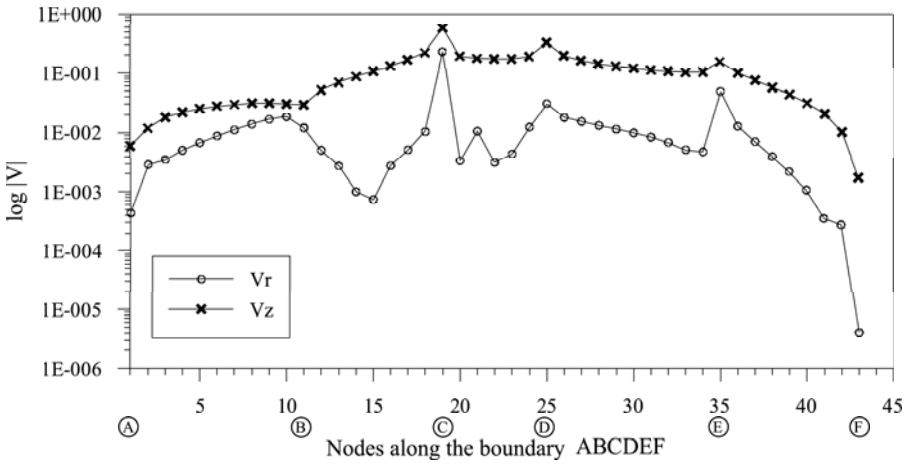

Figure 6.13: Basis **V** along the boundary ABCDEF

Figure 6.14 presents the displacements along the boundary ABCDEF. Displacements and stresses were evaluated at 20 nodes along the segments A'B' and C'D', as shown in Fig. 6.15. Table 6.4 presents the global relative errors for the displacements and stresses evaluated along the boundary and in the domain.

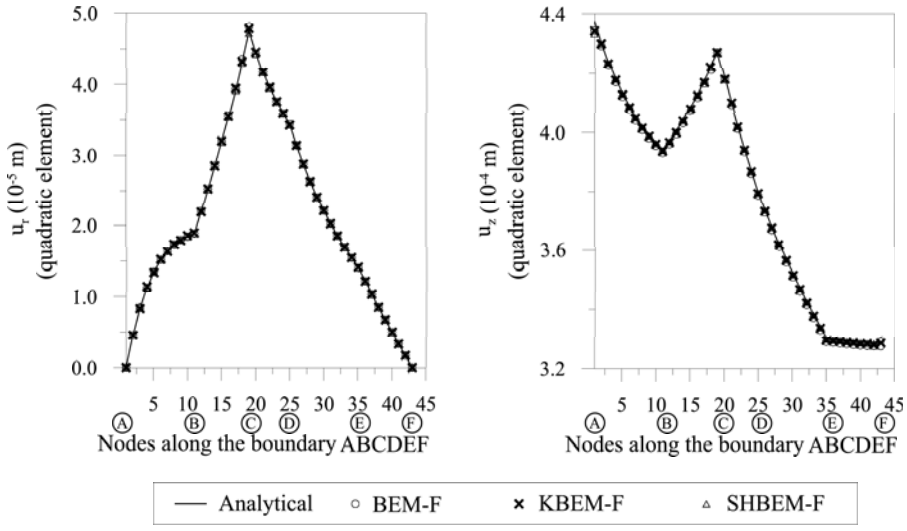

Figure 6.14: Displacements along the boundary ABCDEF

Table 6.4: Global errors of the results found for an irregularly shaped, simply-connected domain subjected to a stress field

Method	**Error (%)** *Along the boundary*		*In the domain*				
	u_r	u_z	u_r	u_z	σ_{rr}	σ_{rz}	σ_{zz}
BEM-F	0.57	0.36	0.05	0.31	0.30	0.41	0.15
KBEM-F	0.43	0.22	0.09	0.15	0.16	0.69	0.17
SHBEM-F	0.33	0.23	0.16	0.02	1.60	13.77	0.81

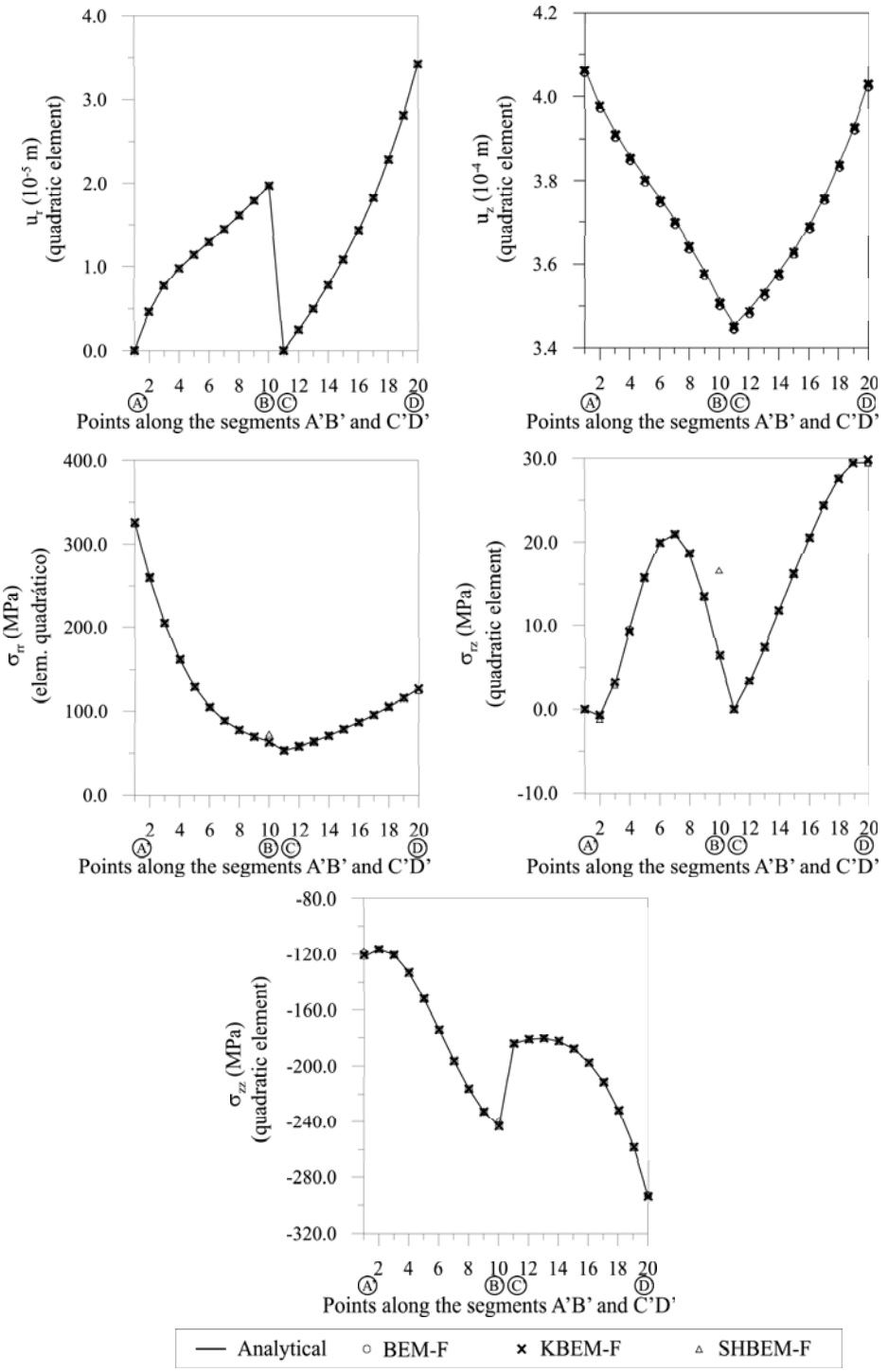

Figure 6.15: Displacements and stresses along the segments A'B' and C'D'

The numerical and analytical results present good agreement. As in the previous example, the global relative error of the stress σ_{rz} in Fig. 6.15 and Table 6.4 for the simplified-hybrid boundary element method (SHBEM-F) is due to the proximity of the internal point B' to the boundary elements, which is not treated adequately in this work. On the other hand, the error for displacements present good accuracy when compared to the error for the boundary element method that

makes use of a stiffness matrix (KBEM).

6.1.5
Irregularly shaped, hollow multiply-connected domain subjected to a stress field

Consider the same boundless elastic medium of the previous example, subjected to a point force $\mathbf{p}^* \equiv (p_r^*, p_z^*) = (1, 1)$ applied at the coordinates P = (10, −5). Now, let an irregular patch be drawn in this elastic medium, as depicted in Fig.6.16, constituting a closed axisymmetric domain that does not contain the force $\mathbf{p}^*$ applied at point P. As in the previous example, one can evaluate the displacements and traction forces along the boundary ABCDEFA by Eqs. (6-5) and (6-6) and use them as target values for comparison with the numerical simulations.

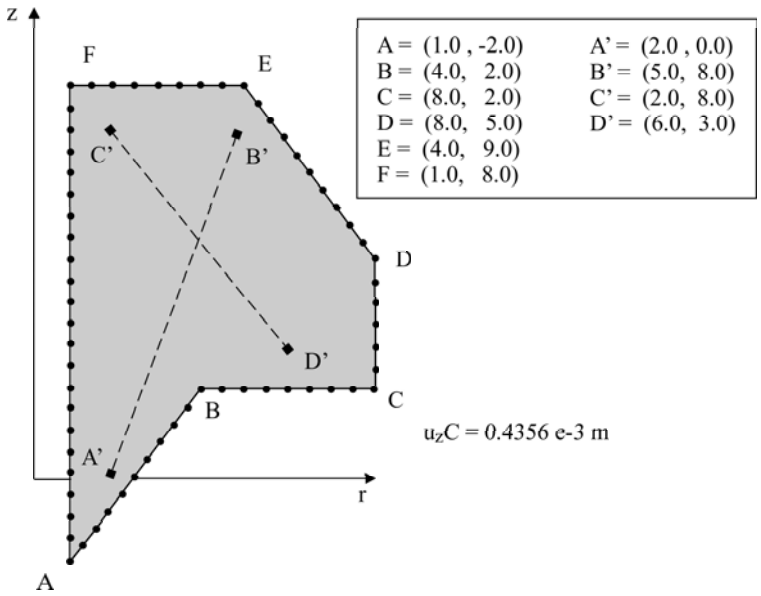

Figure 6.16: Boundary element model of an irregularly shaped, hollow multiply-connected domain subjected to a stress field

Consider the problem of an irregularly shaped domain, depicted in Fig. 6.16, subjected to traction forces along the boundary and prescribed displacement in the z-direction at C, obtained as above outlined. Again, one solves the problem numerically for displacements and compares with the analytical expressions given by Eq. (6-5).

This problem was analyzed by a model with 64 nodes and quadratic elements, as depicted in Fig. 6.16. One may notice in Fig. 6.17 that the basis $\mathbf{V}$ given in Section 4.1.3 has coefficients of small values in the r-direction at the nodes between points A and F, which is consistent with the fact the domain is multiply connected. Again, despite such small coefficients, one could achieve good accuracy in the results with the simplified boundary element method (SHBEM-F) by employing the

procedure proposed in Section 4.1.5 for the evaluation of the unknown coefficients of $\mathbf{U}^*$.

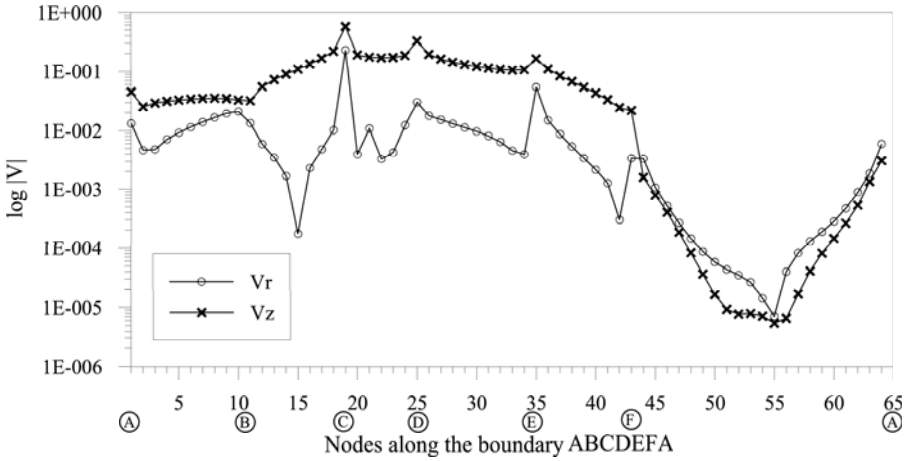

Figure 6.17: Basis $\mathbf{V}$ along the boundary ABCDEFA

Figure 6.18 presents the displacements along the boundary ABCDEFA. Displacements and stresses were evaluated at 20 points along the segment A'B' and C'D', as shown in Fig. 6.19. Table 6.5 presents the global relative errors for the displacements and stresses evaluated along the boundary and in the domain.

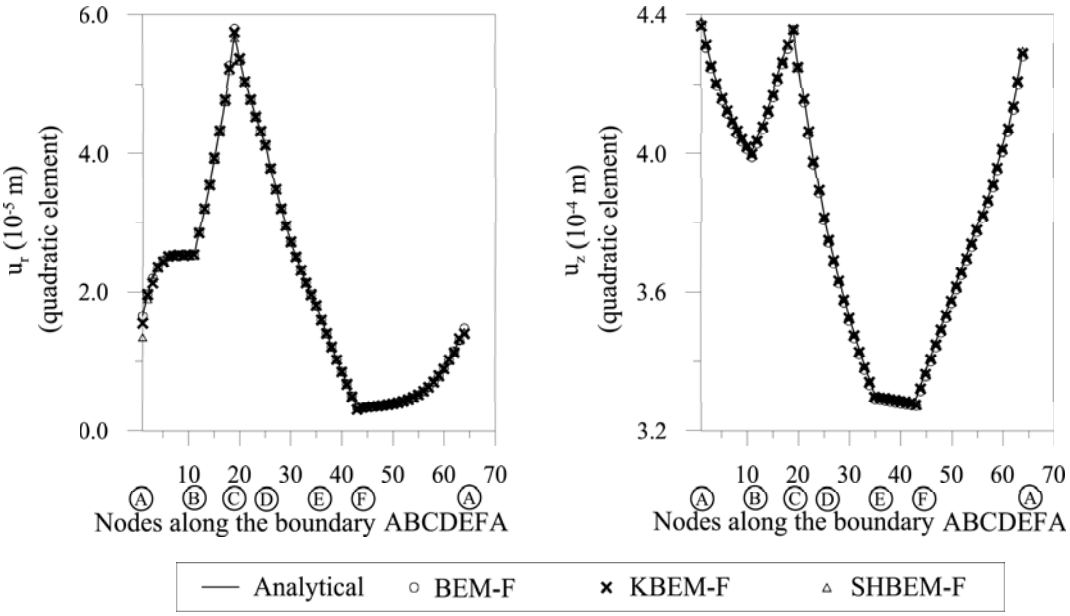

Figure 6.18: Displacements along the boundary ABCDEFA

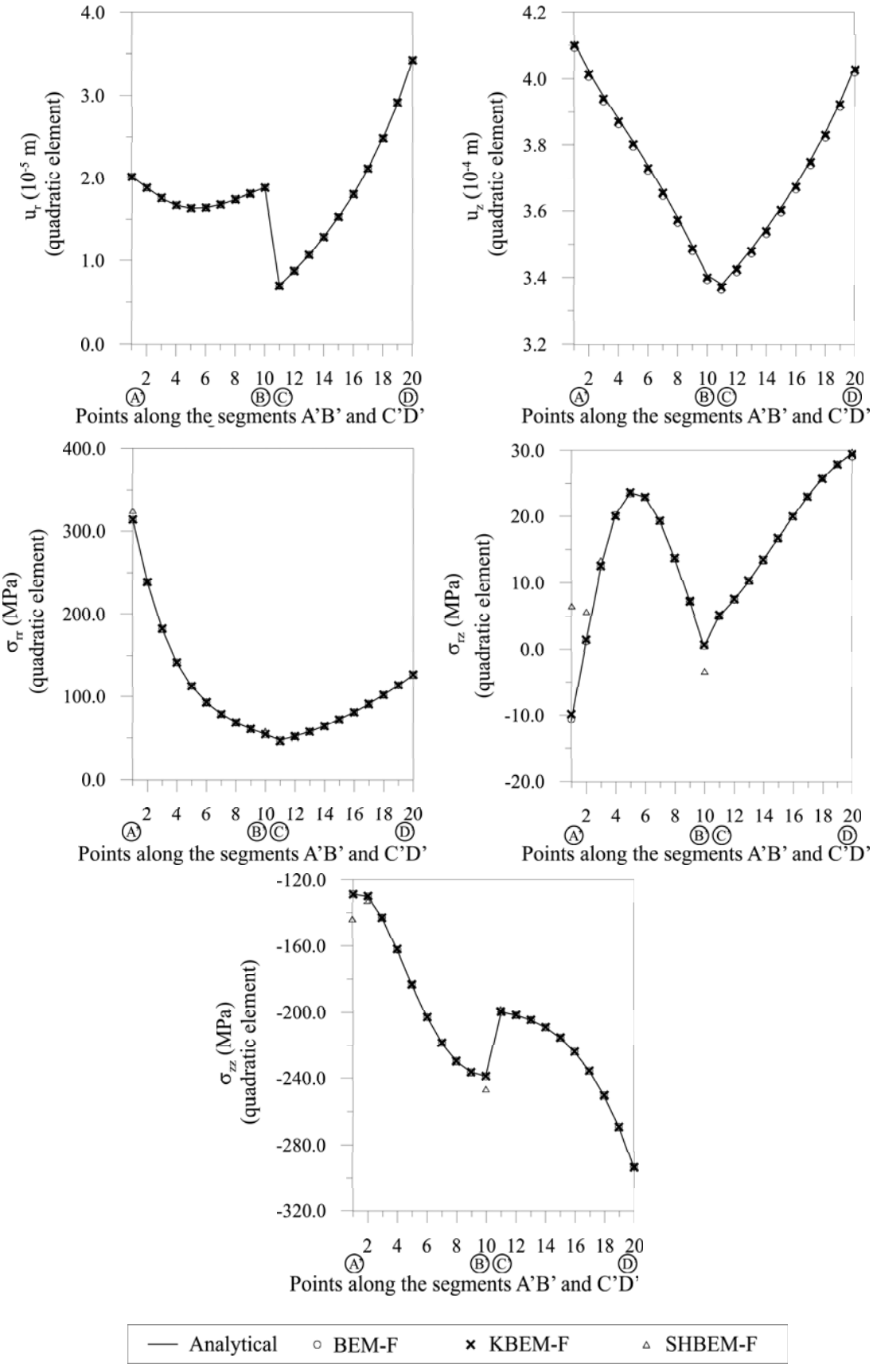

Figure 6.19: Displacements and stresses along the segments A'B' and C'D'

Table 6.5: Global errors of the results found for an irregularly shaped, hollow multiply-connected domain subjected to a stress field

Method	**Error (%)** *Along the boundary*		*In the domain*				
	u_r	u_z	u_r	u_z	σ_{rr}	σ_{rz}	σ_{zz}
BEM-F	0.57	0.29	0.10	0.42	0.12	0.75	0.10
KBEM-F	0.52	0.21	0.13	0.21	0.22	1.55	0.11
SHBEM-F	1.53	0.12	0.04	0.12	2.07	23.28	1.82

The numerical and analytical results present good agreement. As in the previous examples, the global relative error of stresses σ_{rz} in Fig. 6.19 and Table 6.5 for the simplified-hybrid boundary element method (SHBEM-F) is due to the proximity of the internal points A'and B' to the boundary elements, which is not treated adequately in this work. The error for displacements present good accuracy when compared to the error for the boundary element method that makes use of a stiffness matrix (KBEM).

6.2
Problems in an infinite medium

6.2.1
Irregularly shaped, simply-connected cavity subjected to a stress field

In a similar manner to the examples presented in sections 6.1.4 and 6.1.5, consider the force $\mathbf{p}^* \equiv (p_r^*, p_z^*) = (1, 1)$ MN applied at a point P $= (3, -5)$ in the same boundless elastic medium of the previous example. Now, consider the problem of an irregularly shaped cavity, depicted in Fig. (6.20), subjected to traction forces along the boundary and prescribed displacement in the z-direction at C, obtained by Eqs. (6-5) and (6-6) for the appliced forces $\mathbf{p}^*$. One solves the problem numerically for displacements and compares with the analytical results given by Eq. (6-5).

The problem was analyzed by a model with 43 nodes and quadratic elements, as depicted in Fig. 6.20. One might obtains the unknown values of $\mathbf{U}^*$ for the finite, complementary domain, exactly as procedded for the example of Section 6.1.4. However, the same problems reported with reference to the basis $\mathbf{V}$ would appear. Since the procedure proposed in Section 4.1.5 for the evaluation of the unknown coefficients of matrix $\mathbf{U}^*$ does not depend on the basis $\mathbf{V}$, one could achieve good accuracy in the results with the simplified boundary element method (SHBEM-F).

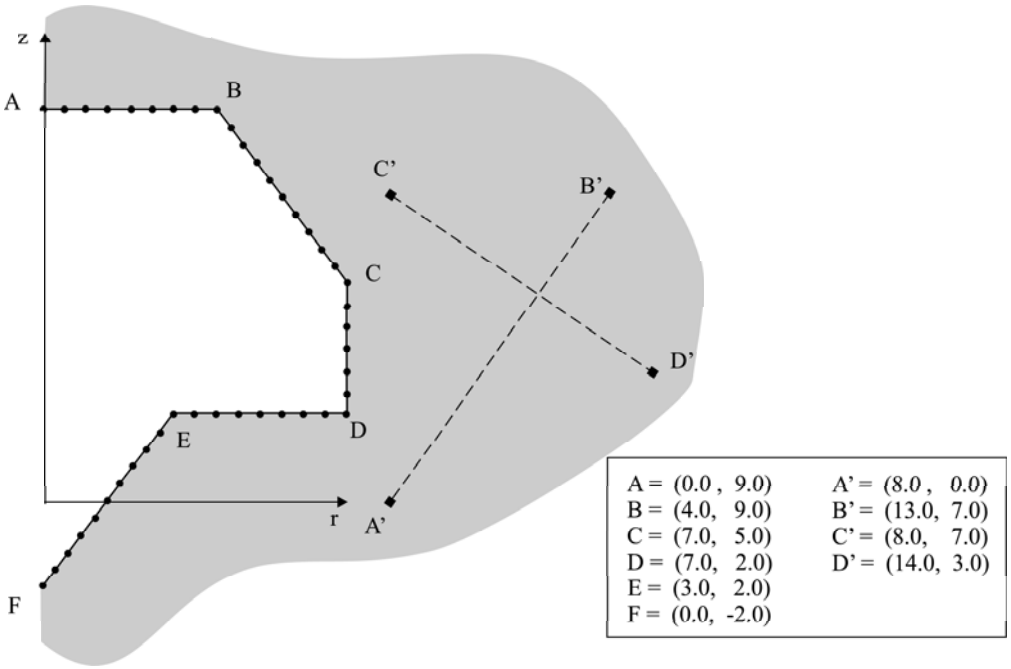

Figure 6.20: Boundary element model of an irregularly shaped, simply-connected cavity subjected to a stress field

The displacements along the boundary ABCDEF are presented in Fig. 6.21. Displacements and stresses were evaluated at 20 internal points along the segments A'B' and C'D', as shown in Fig. 6.22. Table 6.6 presents the global relative errors for the displacements and stresses evaluated along the boundary and in the domain. All the numerical results present excellent agreement with analytical results. Notice that, for this example, all the internal points are located far enough from the boundary elements and the errors for displacements and stresses obtained by the simplified-hybrid boundary element method (SHBEM-F) present very good accuracy.

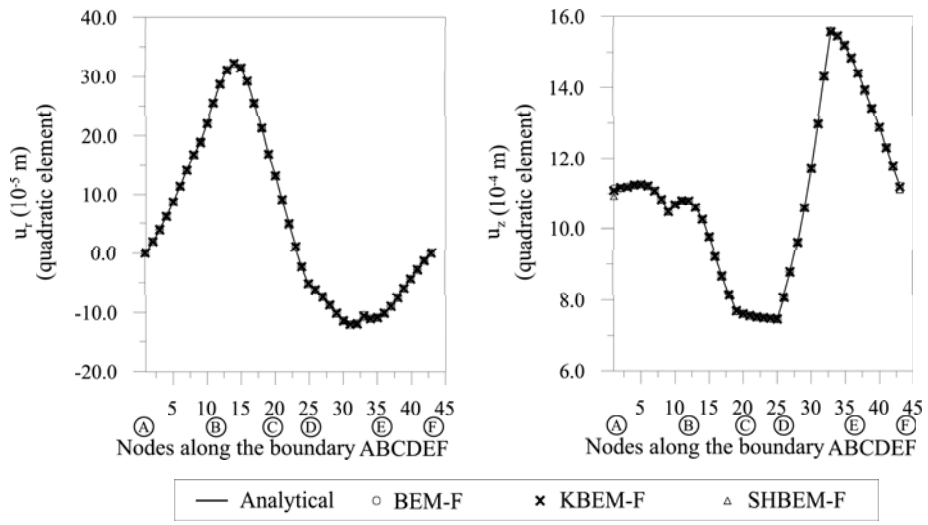

Figure 6.21: Displacements along the boundary ABCDEF

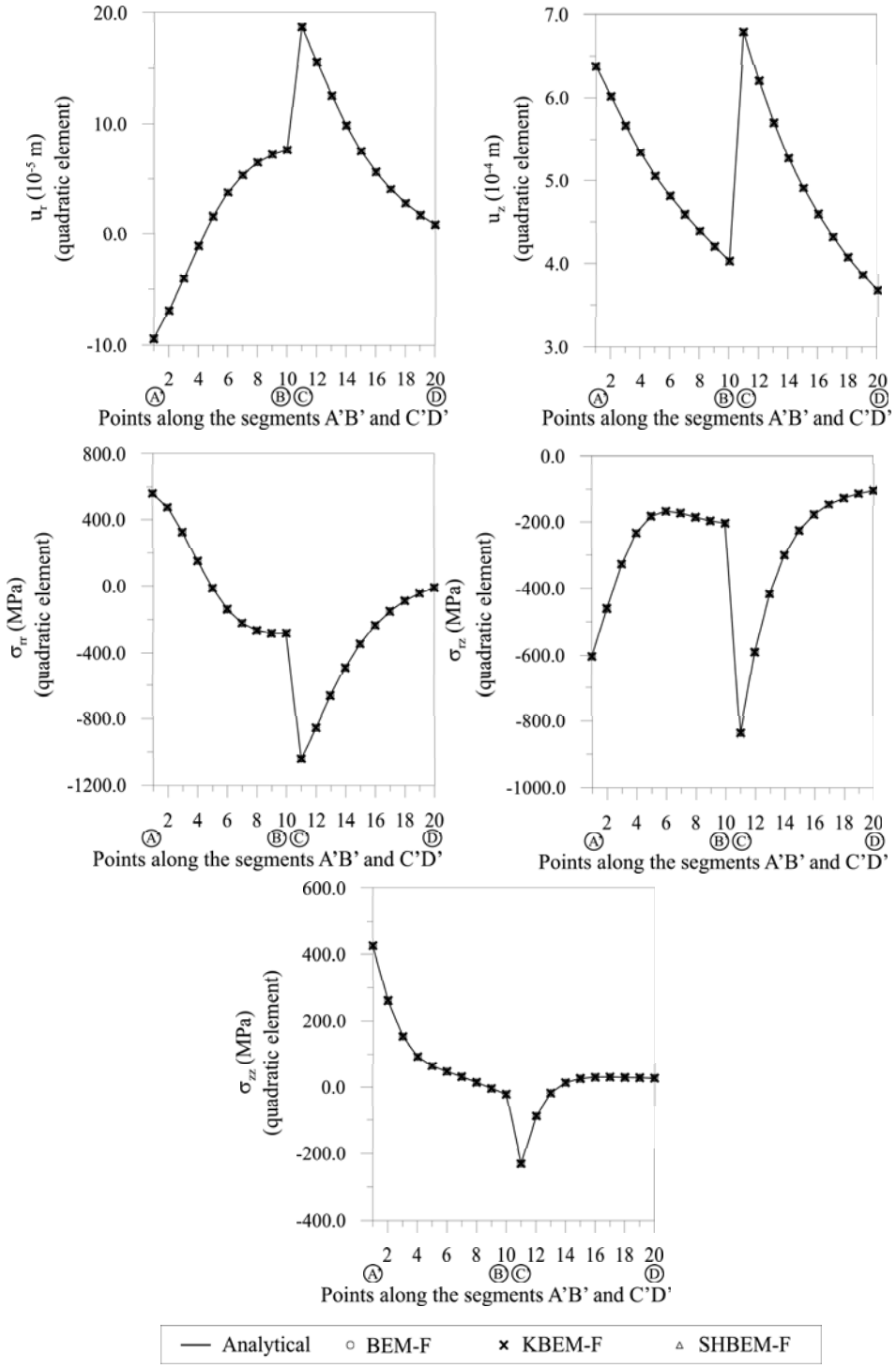

Figure 6.22: Displacements and stresses along the segments A'B' and C'D'

Table 6.6: Global errors of the results found for an irregular simply-connected cavity subjected to a stress field

Method	**Error (%)** *Along the boundary*		*In the domain*				
	u_r	u_z	u_r	u_z	σ_{rr}	σ_{rz}	σ_{zz}
BEM-F	0.07	0.01	0.01	0.00	0.01	0.01	0.01
KBEM-F	0.26	0.12	0.01	0.00	0.02	0.02	0.08
SHBEM-F	0.52	0.38	0.02	0.00	0.03	0.02	0.07

6.2.2
Irregularly shaped, multiply-connected cavity subjected to a stress field

In a similar manner to the previous example, consider the force $\mathbf{p}^* = (1, 1)$ MN applied at a point $\mathrm{P} = (4, 5)$ in the same elastic medium. Now, consider the problem of an irregularly shaped cavity, depicted in Fig. (6.23), subjected to traction forces along the boundary and prescribed displacement in the z-direction at C, obtained by Eqs. (6-5) and (6-6). Once more, one solves the problem numerically for displacements along the boundary ABCDEF and compares with the analytical results given by Eq. (6-5).

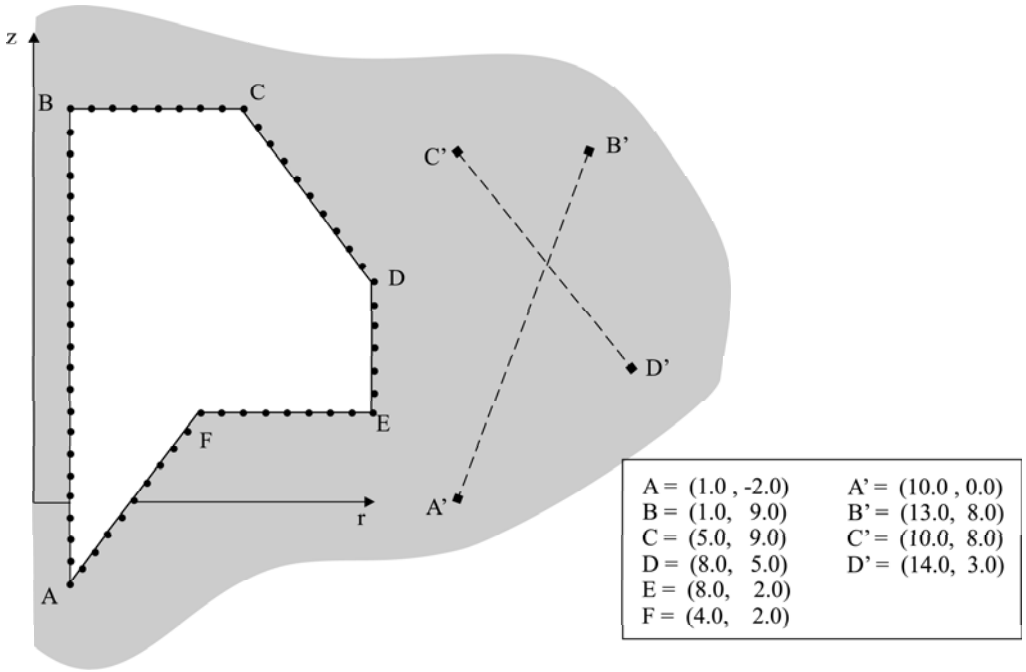

Figure 6.23: Boundary element model of an irregularly-shaped multiply-connected cavity subjected to a stress field

The problem was analyzed using a model with 64 nodes and quadratic elements, as depicted in Fig. 6.23. As in the previous example, the body is a non-convex domain with disconnected surfaces. The basis $\mathbf{V}$ given in Section 4.1.3,

found for the complementary domain, presents the issues reported for the example of Section 6.1.5. Since the procedure proposed in Section 4.1.5 for the evaluation of the unknown coefficients of $\mathbf{U}^*$ does not depend on the basis $\mathbf{V}$, one could achieve good accuracy of the results using the simplified boundary element method (SHBEM-F).

Results along the boundary ABCDEFA and at 20 equally spaced points along the segments A'B' and C'D' are presented in Figs. 6.24 and 6.25, repectively. Table 6.7 presents the global relative errors for the displacements and stresses evaluated along the boundary and in the domain. All the numerical results present excellent agreement with analytical expressions. Notice that, for this example, all the internal points are located far enough from the boundary elements and the errors for displacements and stresses obtained by the simplified-hybrid boundary element method (SHBEM-F) present very good accuracy.

Method	**Error (%)**						
	Along the boundary		*In the domain*				
	u_r	u_z	u_r	u_z	σ_{rr}	σ_{rz}	σ_{zz}
BEM-F	0.09	0.01	0.01	0.00	0.01	0.01	0.01
KBEM-F	0.36	0.14	0.01	0.00	0.02	0.01	0.05
SHBEM-F	0.42	0.07	0.02	0.00	0.03	0.01	0.06

Table 6.7: Global errors of the results found for an irregularly-shaped, multiply-connected cavity subjected to a stress field

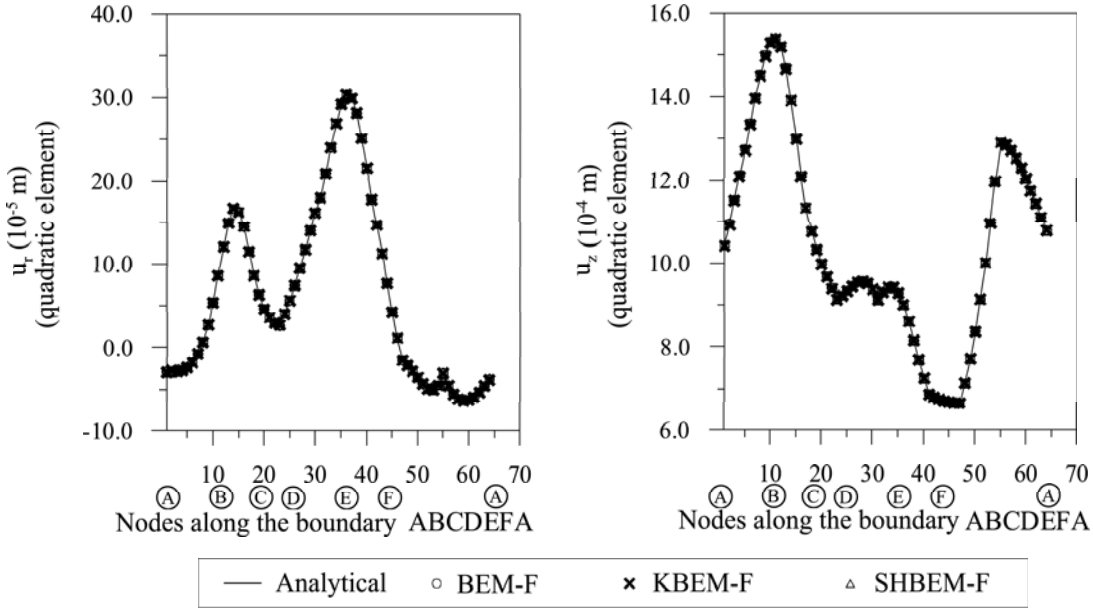

Figure 6.24: Displacements along the boundary ABCDEFA

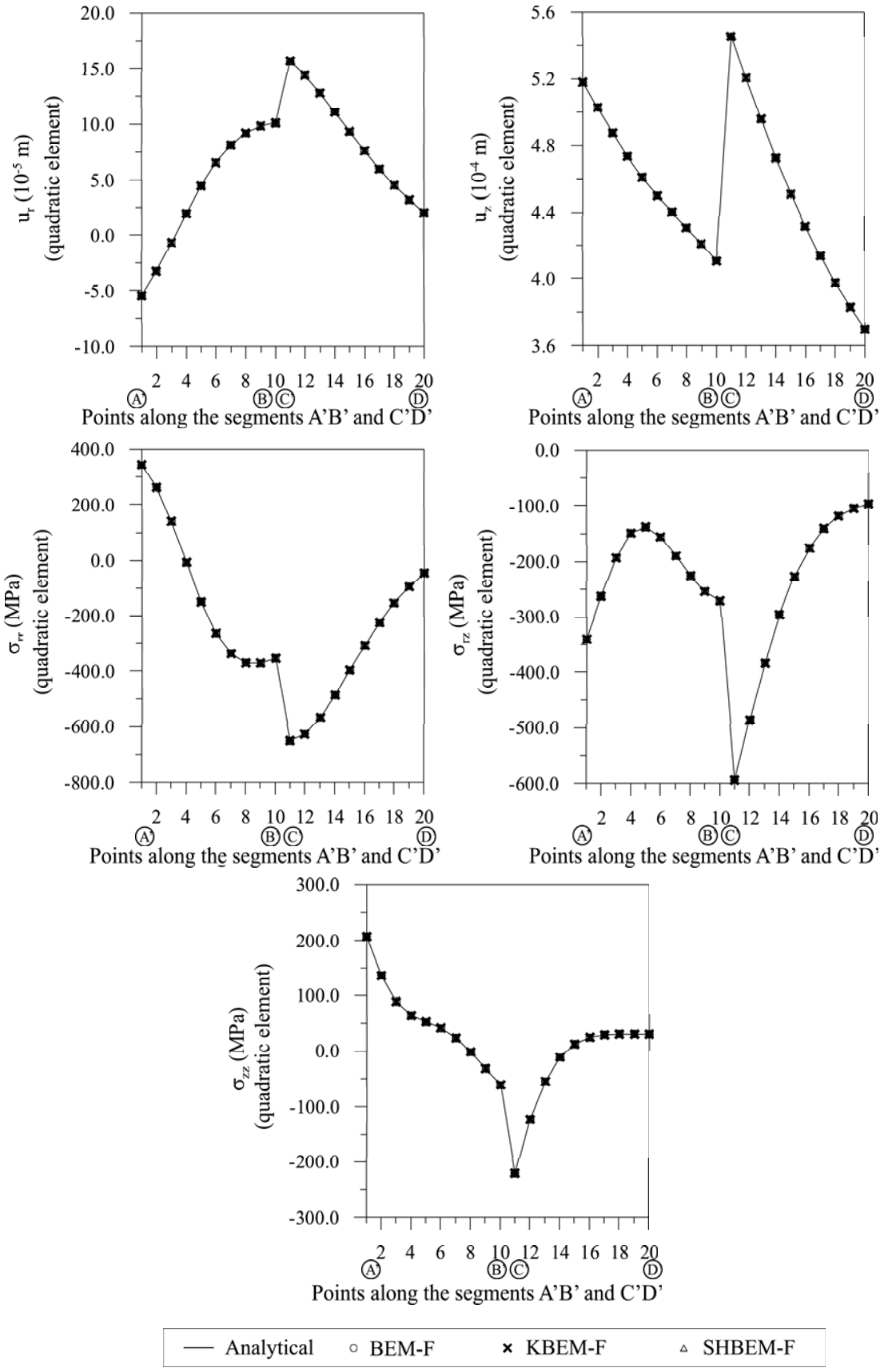

Figure 6.25: Displacements and stresses along the segments A'B' and C'D'

6.3
Problems in the halfspace

6.3.1
Halfspace subjected to a compressive load on the surface

Fig. 6.26 illustrates the halfspace $z \leq 0$ with unitary shear modulus and Poisson's ratio $\nu = 0.25$, submitted to a uniform compressive load on a circle of radius $R = 5m$. The analytical expressions for the vertical displacement and axial stress can be found in Selvadurai [91] and Milovic [92] as

$$u_z = \frac{p\,R}{2\mu}\,[2(1-\nu)\,I_{10-1}(R,r;z) + z\,I_{100}(R,r;z)] \tag{6-7}$$

$$\sigma_{zz} = p\left\{A - \frac{n}{\pi\sqrt{n^1+(1+t)^2}}\left[\frac{n^2+t^2-1}{n^2+(1-t)^2}\,E(k) + \frac{1-t}{1+t}\,\Pi_0(k,q)\right]\right\} \tag{6-8}$$

in which

$$n = \frac{z}{R}, \quad t = \frac{r}{R}, \quad k^2 = \frac{4t}{n^2+(t+1)^2}, \quad q = \frac{4t}{(t+1)^2} \quad \text{e} \tag{6-9}$$

$$A = \begin{cases} 1 & \text{if} \quad r < R \\ 1/2 & \text{if} \quad r = R \\ 0 & \text{if} \quad r > R \end{cases} \tag{6-10}$$

where p is the uniform pressure and the z-axis is positive in the downward direction.

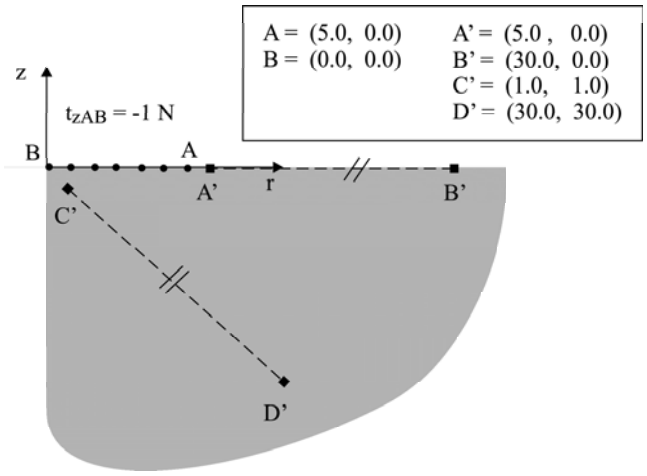

Figure 6.26: Boundary element model of a halfspace subjected to uniform pressure on a circular surface

This problem was analyzed using a model with 7 nodes and quadratic elements, as depicted in Fig. 6.26. The displacements along the boundary AB are shown in Fig. 6.27. The displacement u_z and the stress component σ_{zz} were evaluated at 9 and 14 points equally spaced along the segments A'B' and C'D', respec-

tively, and are shown in Fig. 6.27. Table 6.8 presents the global relative errors for the displacements and stresses evaluated along the boundary and in the domain. All the numerical results present good agreement with analytical expressions. The problem was not solved in terms of a stiffness matrix derived from the simplified-hybrid boundary element method, since the analytical solutions for the halfspace problem as still not available, as presented in Section 4.2.

Actually, the solution of the present problem, with Neumann boundary conditions, is a trivial one in the frame of the hybrid boundary element method, since only the solution of Eq. (4-14) for $\mathbf{p}^*$ is required. Then, all results at internal points would be immediately available, with the best possible accuracy among all boundary element methods, since only approximations related to the matrix **H** are assumed in the numerical simulation.

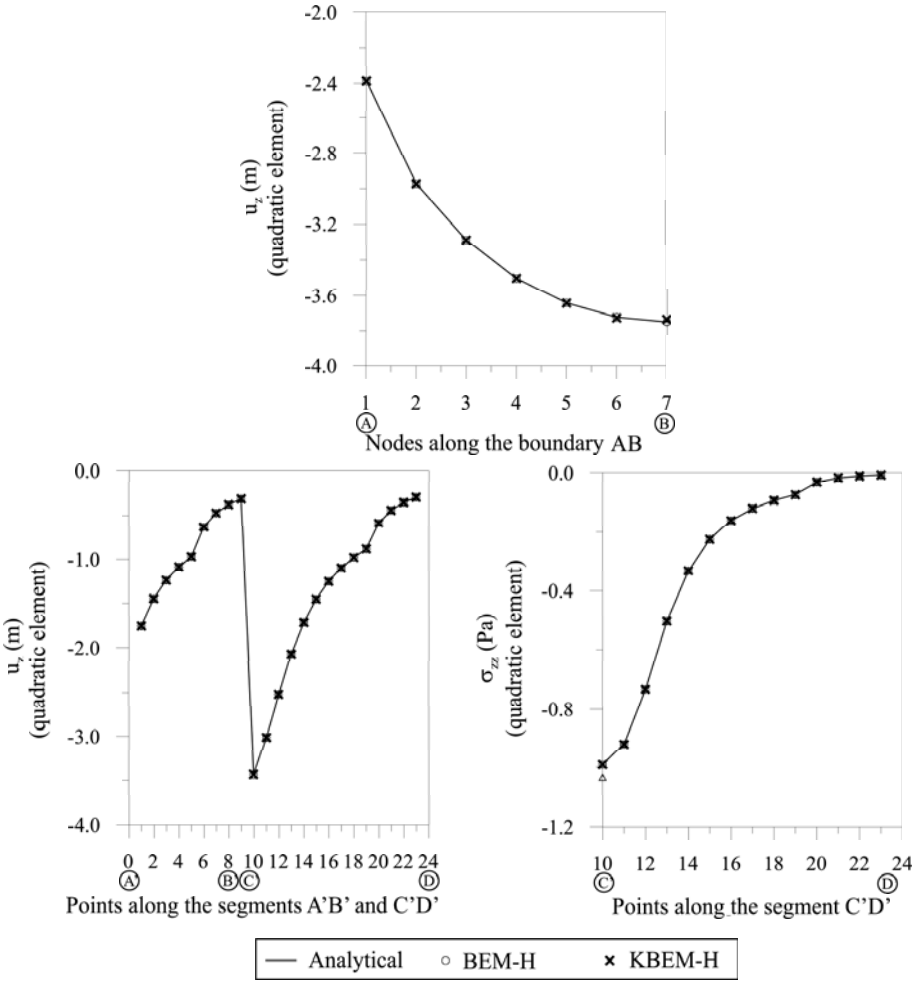

Figure 6.27: Displacements and stresses along the boundary AB and along the segments A'B' and C'D

Table 6.8: Global errors of the results found for a halfspace subjected to compressive load along a circular surface

Method	**Error (%)**				
	Along the boundary		*In the domain*		
	u_r	u_z	u_r	u_z	σ_{zz}
BEM-H	0.00	0.00	0.00	0.00	0.00
KBEM-H	0.45	0.00	0.00	0.00	0.00

6.3.2 Irregularly shaped, simply-connected cavity subjected to a stress field

Consider a point force $\mathbf{p}^* = (1, 1)$ MN applied at the coordinates P $= (3, -5)$ of an elastic halfspace of shear modulus $\mu = 10$ MPa and Poisson's ratio $\nu = 0.3$. The displacement and the stress fields produced at any point Q $= (r, z)$ can be evaluated by directly applying the halfspace fundamental solution

$$u_i = u^{*\mathrm{h}}_{ir}\, p^*_r + u^{*\mathrm{h}}_{iz}\, p^*_z \tag{6-11}$$

$$\sigma_{ij} = \sigma^{*\mathrm{h}}_{ijr}\, p^*_r + u^{*\mathrm{h}}_{ijz}\, p^*_z \tag{6-12}$$

where $u^{*\mathrm{h}}_{im}$ and $\sigma^{*\mathrm{h}}_{ijm}$ are given in Section 2.3. Now, let an irregular patch be drawn in this elastic medium, constituting a cavity that does not enclose the force $\mathbf{p}^*$ applied at point P, as illustrated in Fig.6.28. From Eq. (6-12), one can evaluate the load along the boundary ABCDEF due to $\mathbf{p}^*$ as described above. These results can be used as target values for comparison with the numerical simulations.

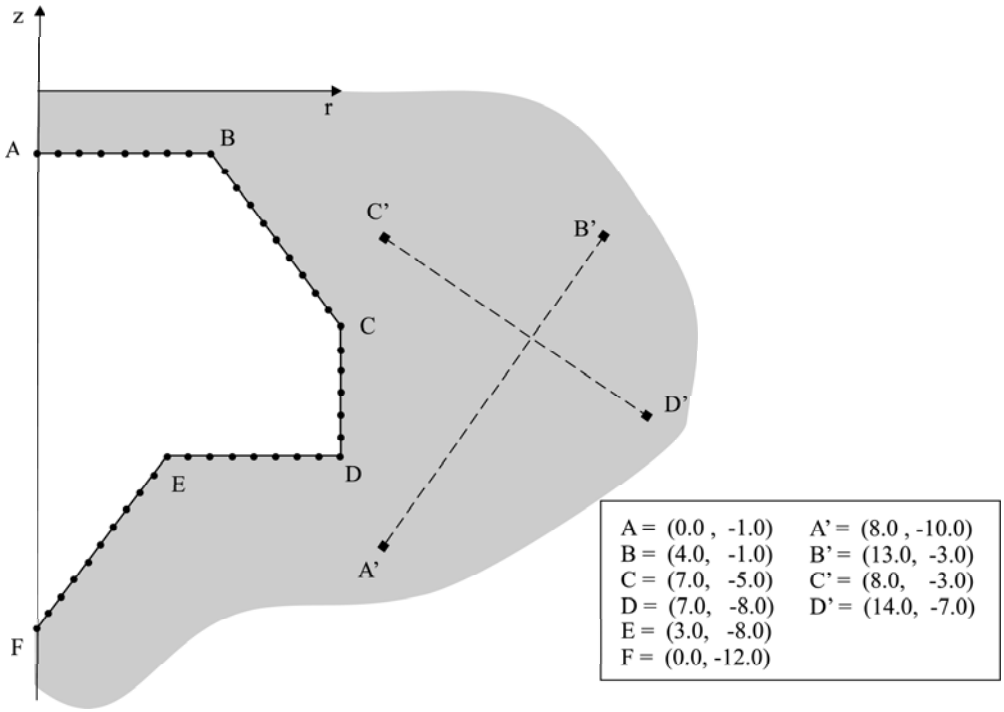

Figure 6.28: Boundary element model of an irregularly shaped, simply-connected cavity subjected to a stress field

Consider the problem of the irregularly shaped cavity, shown in Fig. 6.28, subjected to traction forces along the boundary, as caused by the source $\mathbf{p}^*$. One solves the problem numerically for displacements and compares with the analytical expressions given by Eq. 6-11.

This problem was analyzed by a model with 43 nodes and quadratic elements, as depicted in Fig. 6.28. The displacements along the boundary ABCDEF are shown in Fig. 6.30. The displacements and stresses evaluated at 20 internal points along the segments A'B' and C'D' are presented in Fig. 6.29. Table 6.8 presents the global relative errors for the displacements and stresses evaluated along the boundary and in the domain. All the numerical results present good agreement with the analytical results.

As in the previous example, the problem was not solved in terms of a stiffness matrix derived from the simplified-hybrid boundary element method, since the analytical solutions for the halfspace problem as still not available, as presented in Section 4.2. Actually, the solution of the present problem, with Neumann boundary conditions, is a trivial one in the frame of the hybrid boundary element method, since only the solution of Eq. (4-14) for $\mathbf{p}^*$ is required. Then, all results at internal points would be immediately available, with the best possible accuracy among all boundary element methods, since only approximations related to the matrix $\mathbf{H}$ are assumed in the numerical simulation.

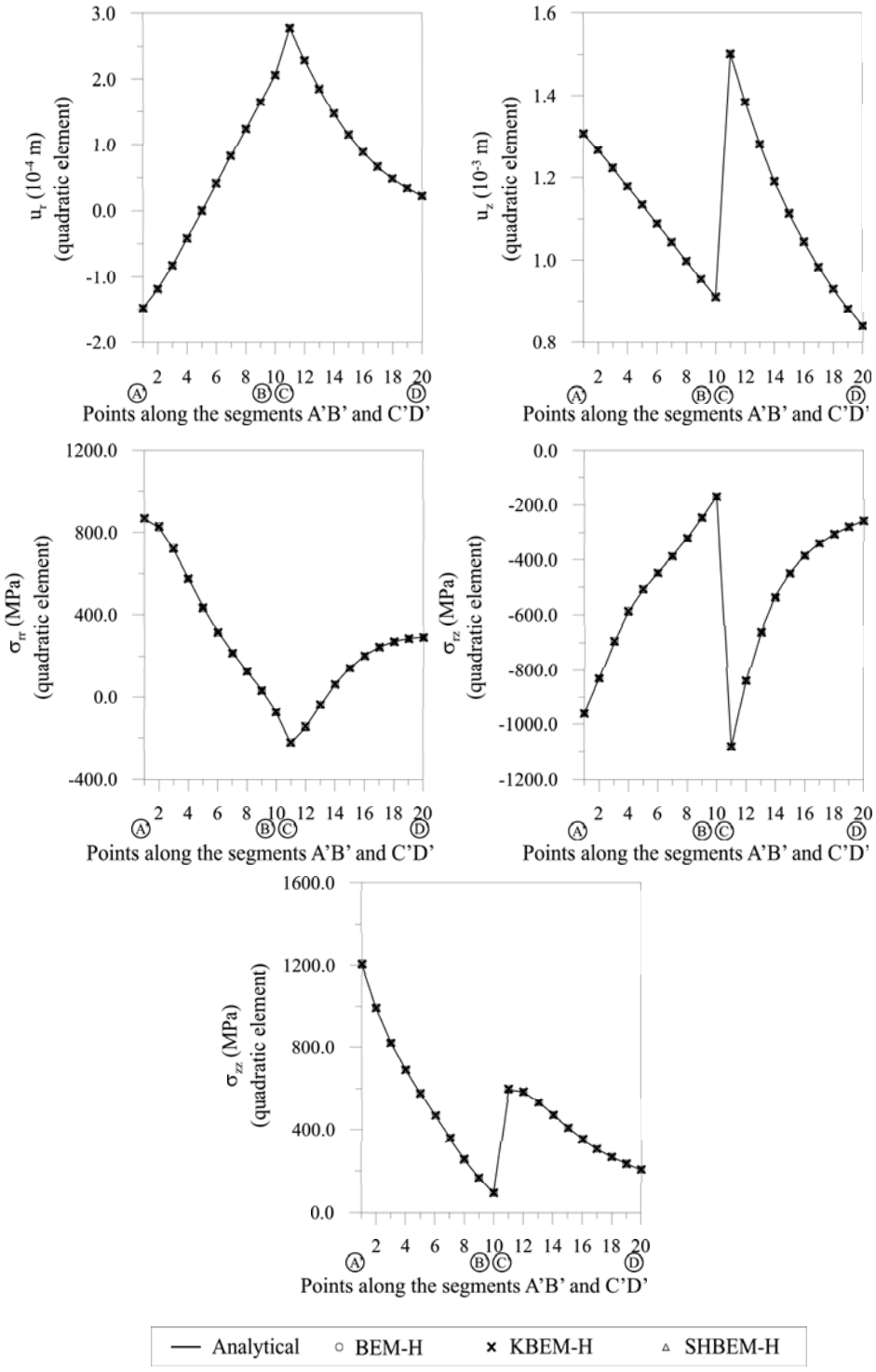

Figure 6.29: Displacements and stresses along the segments A'B' and C'D'

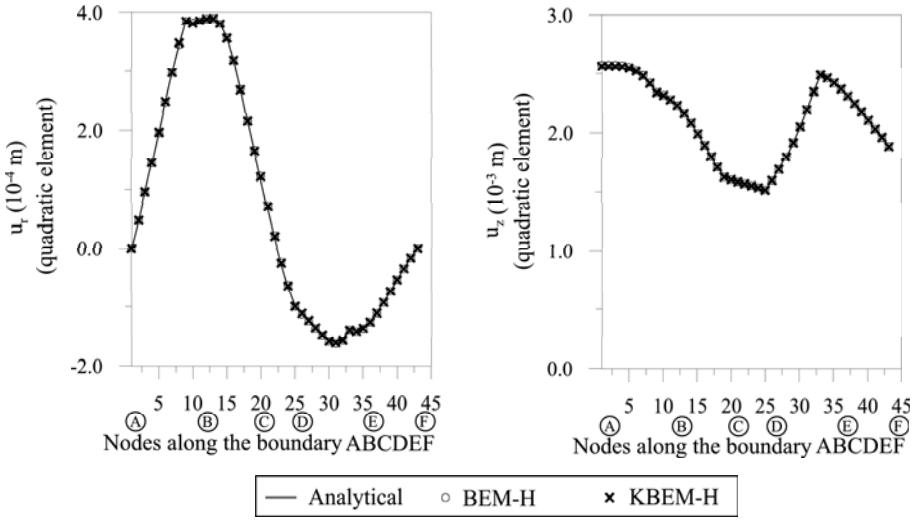

Figure 6.30: Displacements along the boundary ABCDEF

Table 6.9: Global errors of the results found for an irregularly shaped, simply-connected cavity subjected to a stress field

Method	**Error (%)** *Along the boundary*		*In the domain*				
	u_r	u_z	u_r	u_z	σ_{rr}	σ_{rz}	σ_{zz}
BEM-H	1.17	0.35	0.06	1.06	0.45	0.45	0.48
KBEM-H	0.95	0.18	0.03	0.84	0.35	0.35	0.33
SHBEM-H	–	–	0.00	0.03	0.01	0.01	0.02